ADVANCED FUNCTIONAL MATERIALS
www.afm-journal.de

Materials Views
www.MaterialsViews.com

UV-Light-Driven Oxygen Pumping in a High-Temperature Solid Oxide Photoelectrochemical Cell

Georg Christoph Brunauer, Bernhard Rotter, Gregor Walch, Esmaeil Esmaeili, Alexander Karl Opitz, Karl Ponweiser, Johann Summhammer, and Juergen Fleig**

A solid-state photoelectrochemical cell is operated between 400 and 500 °C under 365 nm UV light. The cell consists of a photovoltaic part, based on a $La_{0.8}Sr_{0.2}CrO_3/SrTiO_3$ junction, and an electrochemical part including a zirconia solid electrolyte with a shared (La,Sr)FeO_3 electrode. The photovoltaic cell part leads to open circuit voltages up to 920 mV at 400 °C. Upon UV light, this driving force is used in the electrochemical part of the cell to pump oxygen from low to high partial pressures, i.e., to convert radiation energy to chemical energy. This demonstrates the feasibility of high-temperature photoelectrochemical cells for solar energy storage. The detailed characterization of the different resistance contributions in the system by DC and AC methods reveals the parts of the cell to be optimized for finally achieving high-temperature photoelectrochemical water splitting.

1. Introduction

Exploiting solar energy by solar-to-fuel conversion, i.e., by transferring radiation energy to chemical energy, is of extraordinary relevance for future sustainable energy supply. One approach is based on photovoltaic (PV) cells and subsequent use of electricity in electrolysis cells to generate fuels such as hydrogen, CO, or even hydrocarbons.[1–3] Integration of the photovoltaic part into one electrode of an electrochemical (EC) cell is also an option.[4] Alternatively, direct transfer of solar energy to chemical energy is possible in photo(electro)chemical cells.[5–12] By illuminating photochemically active materials such as TiO_2, water splitting and thus hydrogen production takes place without preceding photovoltaic electricity generation. Either oxygen and hydrogen generation take place at one and the same material, or the corresponding reactions are separated to two electrodes of photoelectrochemical (PEC) cells. Such solar to fuel conversion systems are based on liquid water and despite being heavily investigated, high efficiencies together with high system stability have not been achieved yet.[8,10–12]

Thermochemical energy conversion based on high-temperature materials is a third approach and generally employs two step processes with oxygen release (i.e., a reduction reaction) at high temperature and chemical water splitting at lower temperatures.[13–17] Interestingly, only very few activities aim at a combination of high temperatures and photoelectrochemical energy storage. In a theoretical paper, a solid-state electrochemical cell was suggested for splitting of steam at high temperatures by solar radiation.[18] Such a high-temperature cell running on steam may avoid stability problems of photoactive materials in liquid water, can exploit the reduced theoretical energy input required for water splitting at higher temperatures, and does not suffer from problems due to heating in case of high solar energy intensity. However, to the best of the authors' knowledge, experimental realization of solid electrolyte-based (photo-) electrochemical cells for photon-driven steam electrolysis has not been reported yet.

The scope of this paper is to experimentally demonstrate the feasibility of a high-temperature solid-state photoelectrochemical cell (SOPEC). The multilayer cell used consists of a sequence of different oxides, some being active in terms of photovoltaics and some using the voltage to chemically store energy. At operating temperatures between 400 and 500 °C UV light-induced open circuit voltages as high as 900 mV are directly transferred into chemical energy via oxygen pumping from low to high oxygen partial pressure. The experiments show that solid-state photoelectrochemical cells can indeed be realized and that improved cells for water splitting and thus hydrogen production are feasible.

2. The High-Temperature Photoelectrochemical Cell

The SOPEC investigated in this study is sketched in **Figure 1**a. It includes a thin layer of $La_{0.8}Sr_{0.2}CrO_3$ (LSCr) deposited on a nominally undoped $SrTiO_3$ (100) single crystal; a scanning

G. C. Brunauer, B. Rotter, E. Esmaeili, Prof. K. Ponweiser
Institute for Energy Systems and Thermodynamics
Getreidemarkt 9 E302, 1060 Vienna, Austria
E-mail: georg.brunauer@tuwien.ac.at
G. C. Brunauer
NOVAPECC GmbH
Opernring 19, 1010, Vienna Austria
G. Walch, Dr. A. K. Opitz, Prof. J. Fleig
Institute of Chemical Technologies and Analytics
Getreidemarkt 9 E164-EC, 1060 Vienna, Austria
E-mail: juergen.fleig@tuwien.ac.at
Prof. J. Summhammer
Institute of Atomic and Subatomic Physics
Stadionallee 2 E141, 1020 Vienna, Austria

DOI: 10.1002/adfm.201503597

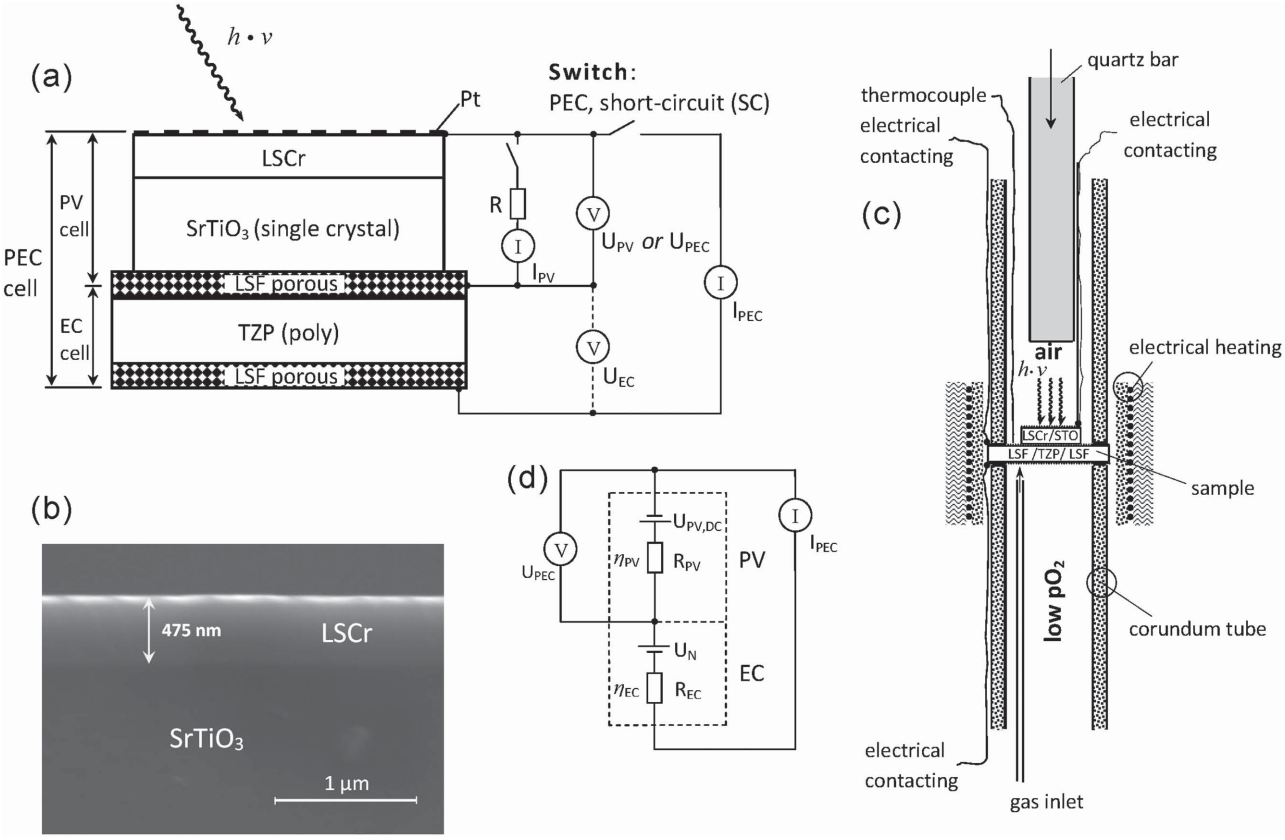

Figure 1. a) Sketch of the investigated solid oxide PEC cell and the measurement arrangement. b) SEM cross section image of a 20% Sr doped $LaCrO_3$ (LSCr) layer on a (100) $SrTiO_3$ single crystal. c) Sketch of the entire setup for investigating the photoelectrochemical cell with two different gas chambers. d) Circuit representing the entire PEC cell. Both the PV and EC part are represented by an ideal battery with internal resistance. The PV "battery" with voltage $U_{PV,OC}$ operates only under illumination and the Nernst voltage U_N is only effective for asymmetric gas supply.

electron microscopy (SEM) cross section image of such a LSCr layer on $SrTiO_3$ is shown in Figure 1b. A thin film Pt current collector grid is used on top of LSCr. The $SrTiO_3$ single crystal with top layers is attached to a symmetrical solid-state electrochemical cell with porous $La_{0.6}Sr_{0.4}FeO_{3-\delta}$ (LSF) electrodes on a tetragonal zirconia polycrystal (TZP). Hence, the entire cell—in the following denoted as PEC cell—can be divided into two parts: a PV part consisting of LSCr/$SrTiO_3$/LSF and an EC part including LSF/zirconia/LSF. One LSF electrode acts as shared electrode, i.e., as top electrode of the EC cell and bottom electrode of the PV cell.

This PEC cell is mounted in a tube furnace such that two different gas compartments result, see Figure 1c. At temperatures between 400 and 500 °C, the PEC cell is illuminated by UV light (365 nm) and the electrical performance is investigated, together with chemical effects (oxygen pumping monitored by oxygen partial pressure changes). Voltages are always measured between the LSCr top electrode and the shared LSF electrode, either without connection between top and PEC cell bottom electrode (then indicated by symbol U_{PV}) or with an external short circuit (SC), i.e., under PEC operating conditions (denoted U_{PEC}), see Figure 1a. In the latter case, the voltage of the EC cell part (U_{EC}) equals the measured voltage U_{PEC} due to the external short circuit, i.e., U_{PEC} (=U_{PV}) = U_{EC} (all voltages with positive sign). Currents are either I_{PEC} indicating the short-circuit current of the entire PEC cell or I_{PV} when only investigating the PV part of the cell. A simplified electrical representation of the PEC cell is shown in Figure 1d. It includes internal resistances of both cell parts and the ideal voltages occurring in the cell, a photovoltaic voltage $U_{PV,OC}$ of the illuminated cell and a Nernst voltage U_N of the electrochemical cell with asymmetric gas supply. This model helps understanding the experiments but is far from being complete; particularly it excludes a detailed representation of the PV cell (internal diode, etc.) and nonlinearities of the EC cell.

3. Results and Discussion

3.1. UV-Light-Driven Oxygen Pumping in the Solid State Photoelectrochemical Cell

When illuminating the PEC cell under open circuit condition, a temperature dependent voltage $U_{PV,OC}$ can be measured at the PV cell. **Figure 2**a,c displays the fast emergence of the voltage at 400 and 500 °C after switching the UV light on. This open circuit voltage with negative polarity at the LSCr electrode is highest at 400 °C (920 mV) and decreases to 630 mV at 500 °C. All values are summarized in **Figure 3**a. Short-circuiting the PV cell leads to currents $I_{PV,SC}$ in the mA range. The highest value

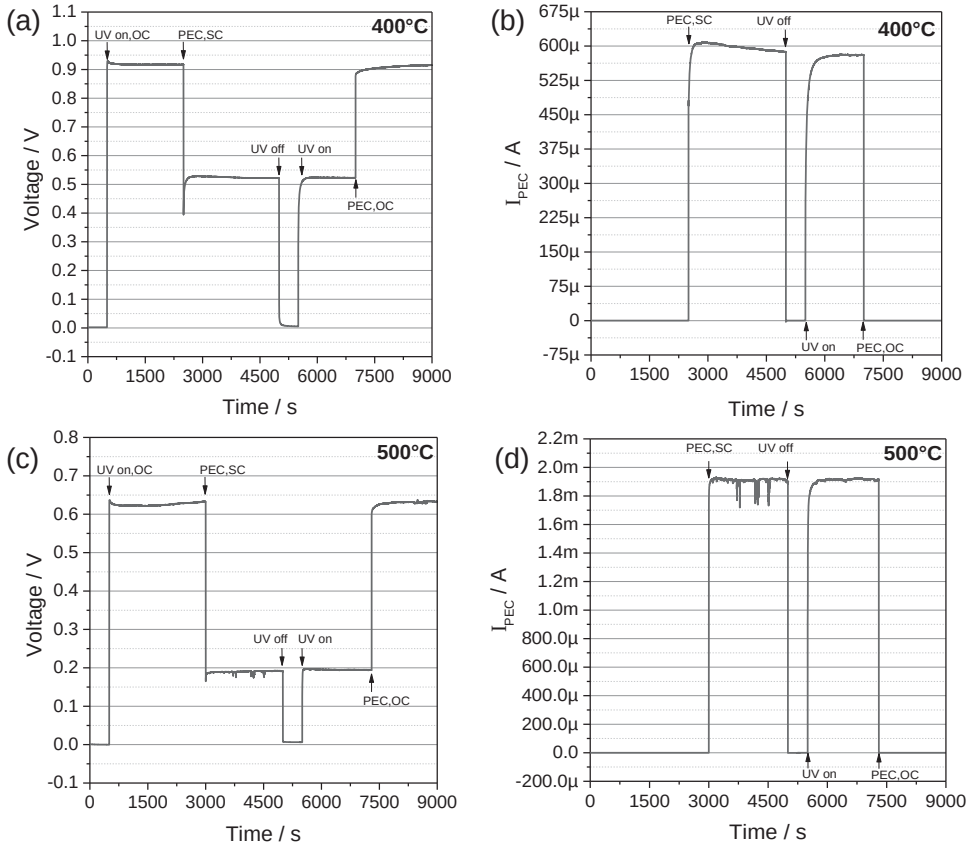

Figure 2. a,c) Open circuit voltage ($U_{PV,OC}$) after switching UV on and voltage under working condition of the PEC cell (U_{PEC}) after short-circuiting the illuminated PEC cell at 400 °C a) and 500 °C c) in symmetric gas atmospheres, $T = T_{dark}$, UV on–off is indicated. b,d) Corresponding current of the PEC cell (I_{PEC}).

of 2.3 mA is found at 500 °C, all measured currents are summarized in Figure 3b. From this we conclude that the $SrTiO_3$ single crystal together with the Sr doped $LaCrO_3$ (LSCr) top electrode acts as an oxide photovoltaic cell with large voltages up to temperatures as high as 500 °C. Another high-temperature solar cell based on Nb-doped $SrTiO_3$ was described by Horkiki et al.[19] but voltages were much smaller in that case. The large voltage found in our cell is the basis of the light-to-chemical energy conversion established here.

When short-circuiting the top (LSCr) and bottom (LSF) electrode of the illuminated PEC cell with symmetrical gas exposure (ambient air at both sides), the measured voltage U_{PEC} drops to 0.19–0.52 V (depending on temperature) and a short-circuit current up to 1.9 mA flows in the cell, see Figure 2b,d.

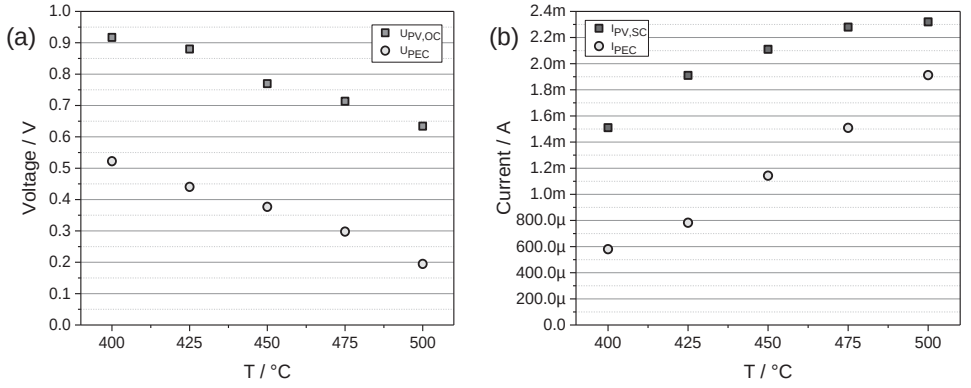

Figure 3. a) PV cell open circuit voltages ($U_{PV,OC}$) and voltages U_{PEC} of the operating PEC cell at temperatures from 400 to 500 °C ($T = T_{dark}$) in symmetric gas atmospheres. b) Short-circuit currents of the PV cell solely ($I_{PV,SC}$) and of the PEC cell (I_{PEC}) at temperatures from 400 to 500 °C in symmetric gas atmospheres.

Relating this current to the electrode area of the electrochemical cell (1.8 cm^2) leads to a current density of ≈1 mA cm^{-2}. The exact voltages U_{PEC} and currents I_{PEC} of the operating PEC cell are summarized in Figure 3a,b. The short-circuit current I_{PEC} has to be ionic in the zirconia electrolyte and thus electrochemical reactions have to take place at the two LSF electrodes of the illuminated PEC cell. In the given cell this is $1/2\ O_2 + 2e^- \Rightarrow O^{2-}$ at the bottom LSF electrode and the reverse reaction at the shared LSF electrode. Provided the voltage U_{PEC} is sufficiently large, this could even allow photoelectrochemical water splitting. Recently, it was experimentally shown that in accordance with Nernst's equation splitting of gaseous water with measurable quantities of hydrogen generation may take place already at voltages much lower than the standard decomposition voltage of water, in that specific study already at ≈600 mV.[20]

In our study, however, the voltage of the short-circuited cell (U_{PEC}) is still somewhat lower. Hence, oxygen pumping against a higher oxygen partial pressure rather than water splitting is employed to demonstrate the potential of the PEC cell for radiation energy to chemical energy conversion. Accordingly, illumination of the PEC cell is also performed for asymmetric gas supply, i.e., for the PV cell being in air and the bottom part of the EC cell being in nitrogen with ≈600 ppm remaining oxygen (measured by an oxygen sensor). The PV cell is not affected by the gas change in the bottom compartment, but the EC cell now exhibits an open circuit voltage of 92–98 mV, depending on temperature (**Figure 4**a,d). This is in accordance with the expected Nernst voltage U_N between ambient air and 600 ppm O_2 (96.8 mV at 500 °C). Upon illumination under short-circuit condition, again a substantial voltage U_{PEC} and a current I_{PEC} up to 1 mA at 500 °C are found (Figure 4b,e).

The measured short-circuit current I_{PEC} leads to pumping of oxygen from the low partial pressure side (oxygen fraction, fo_2, of ≈600 ppm O_2 in 1 bar gas) to the high partial pressure side (≈20% O_2 in 1 bar gas). Figure 4c,f shows that the oxygen content in the low pressure compartment, measured by the oxygen sensor at the outlet, substantially decreases upon UV light. An oxygen fraction of 480 ppm is reached at 400 °C and almost 300 ppm at 500 °C. The correlation between measured current and oxygen pumping becomes clear from the almost linear relation between current and oxygen fraction change Δfo_2 (in ppm), see **Table 1**. Obviously, UV driven oxygen pumping indeed takes place and thus transfer of radiation energy to chemical energy. To the best of our knowledge, this is the first experimental demonstration of a light-driven reaction in a high-temperature solid-state electrochemical cell.

Compared to symmetrical gas condition, voltages U_{PEC} are larger and short-circuit currents I_{PEC} are smaller, cf. Figures 3 and 4. This is straightforward to understand: Owing to negligible gas composition changes in a PEC cell with symmetrical gas supply (air on both sides), the voltage $U_{PEC} = U_{PV}$ of the short-circuited PEC cell is entirely consumed to drive the oxide ion current through the EC cell. Hence, U_{EC} (=U_{PV}) is the sum of all overpotentials η_{EC} in the EC cell, i.e., of anodic, cathodic, and ohmic overpotentials. The difference between $U_{PV,OC}$ and U_{PEC}, on the other hand, is the voltage loss in the PV cell (η_{PV}) and can be associated with its internal resistance ($\eta_{PV} = U_{PV,OC} - U_{PEC}$). When an additional Nernst voltage U_N comes into play due to different gas compositions in the two cell compartments, U_{EC} is no longer given by the internal overpotential of the EC cell solely, but reads

$$U_{EC} = U_{PEC} = U_N + \eta_{EC} \quad (1)$$

Therefore, U_{EC} is increased in the asymmetrical cell. The voltage remaining in the PV cell (η_{PV}), on the other hand, is decreased in accordance with

$$U_{PV,OC} = \eta_{PV} + \eta_{EC} + U_N \quad (2)$$

The corresponding voltages are also indicated in Figure 1d: Under short-circuit condition, the ideal open circuit voltage of the PV cell does not only drive a current across the two internal resistances R_{PV} and R_{EC}, but has also to overcome the Nernst voltage U_N. I_{PEC} is thus lower than for symmetrical gas supply.

For a quantitative estimate of the gas composition change upon UV illumination, we can relate the pumping current I to a molar flux jo_2 of oxygen molecules by

$$j_{O_2} = \frac{1}{4F} I \quad (3)$$

and correlate this with the gas flow rate Q_{gas}; F denotes Faraday's constant. For ideal gases and gas pressure p_{gas} we get the molar gas flux

$$j_{gas} = Q_{gas} \frac{p_{gas}}{RT} \quad (4)$$

Lowering the O_2 fraction in the gas by Δfo_2 corresponds to a current-driven molar oxygen flux of

$$j_{O_2} = j_{gas} \Delta f_{O_2} = Q_{gas} \frac{p_{gas}}{RT} \Delta f_{O_2} \quad (5)$$

and according to Equation (3) to a current of

$$I = \frac{4F}{RT} Q_{gas} p_{gas} \Delta f_{O_2} \quad (6)$$

For Q_{gas} = 10 mL min^{-1}, p_{gas} = 1 bar, and Δfo_2 of 290 ppm at 500 °C we get 290 µA. This is lower than the measured short-circuit current (≈1 mA) but still sufficiently close to be considered as realistic: In our estimate, a constant oxygen partial pressure in the entire compartment was assumed even under pumping condition, which is hardly the case. Inhomogeneities (also in combination with the unknown location of small gas leakage(s) which increase the O_2 content in the N_2 stream) may easily cause the larger pumping current found in the experiment.

3.2. Characterization of the High-Temperature Photovoltaic Cell and the Electrochemical Cell

For a better understanding of our solid oxide photoelectrochemical cell, we characterized the PV part of the PEC cell by determining its *I–V* curves under illumination, i.e., measuring U_{PV} and I_{PV} for different loads and temperatures (**Figure 5**). As already discussed, the open circuit voltage $U_{PV,OC}$ decreases with increasing temperature, while the short-circuit current $I_{PV,SC}$ increases. Hence, the maximum power output is rather temperature independent at 0.33–0.45 mW between 400 and 500 °C. A detailed mechanistic understanding of the

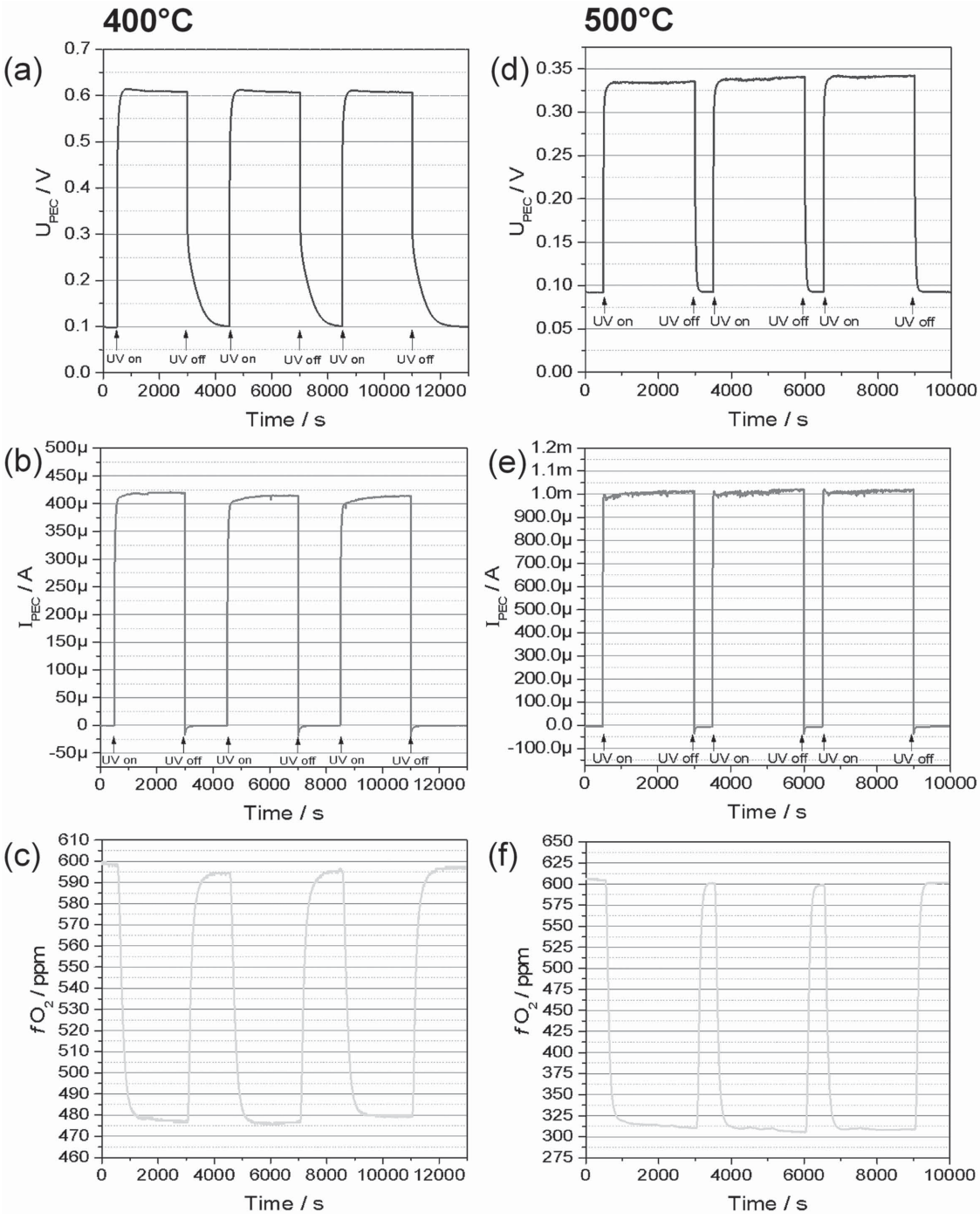

Figure 4. Results of the photoelectrochemically driven oxygen pumping experiment performed in asymmetric gas atmospheres at 400 °C (top) and 500 °C (bottom), $T = T_{dark}$, UV on–off is indicated. a,d) Voltage U_{PEC} of the cell with an open circuit voltage before UV on close to 100 mV due to asymmetric gas atmospheres. b,e) Current I_{PEC} upon UV light under short-circuit condition. c,f) Upon UV light, the oxygen fraction fo_2 in the gas chamber is lowered from 600 to 480 ppm at 400 °C and 310 ppm at 500 °C.

PV cell and its I–V curve is beyond the scope of this paper; it may include not only the photoactive junction but also an ohmic and an additional nonlinear serial resistive contribution. However, we can empirically evaluate the temperature dependent resistance of the PV cell part in the operating PEC cell from

$$R_{PV,PEC} = \frac{\eta_{PV}}{I_{PV}} = \frac{U_{PV,OC} - U_{PV}}{I_{PV}} \quad (7)$$

The resulting values in the several 100 Ω range decrease with increasing temperature and are plotted in **Figure 6**a. Alternatively, we may determine approximate differential resistances by

Table 1. Decrease of the oxygen content in the gas flow at different temperatures and the current of the PEC cell, $T = T_{dark}$.

Temperature [°C]	Change of oxygen content Δfo_2 [ppm]	Current I_{PEC} [μA]
400	120	410
450	240	830
500	290	1000

linearizing the *I–V* curves in Figure 5. This was done for short-circuiting conditions (i.e., $R_{PV,diff} = 50\ mV/(I_{PV,SC} - I_{PV,50mV})$) and the corresponding resistances are also shown in Figure 6a: Values between 417 and 833 Ω are found, in reasonable agreement with $R_{PV,PEC}$.

For further information, impedance spectra were measured on the PV cell part under dark condition and during illumination. In the complex impedance plane the spectrum of the dark PV cell consists of a high frequency arc, an intermediate frequency "shoulder" and a huge low frequency arc. The capacitance of the high frequency arc is close to a typical bulk capacitance of $SrTiO_3$. The resistance of this semicircle is attributed to electronic charge transport in the $SrTiO_3$ single crystal. The corresponding conductivity is strongly temperature dependent (2.38×10^{-6} S cm^{-1} at 400 °C, 8.33×10^{-6} S cm^{-1} at 450 °C and 2.50×10^{-5} S cm^{-1} at 500 °C), in accordance with literature (hole conduction with deep hole traps).[21–23] The impedance spectrum obtained for a $SrTiO_3$ single crystal with a Pt electrode instead of a LSCr electrode (**Figure 7**a, inset) indicates that the intermediate frequency feature can most probably be attributed to the LSF electrode.

Accordingly, the very pronounced low frequency arc of the PV cell reflects the $SrTiO_3$/LSCr interface, i.e., a space charge zone with strong depletion of the main charge carrier (holes in undoped $SrTiO_3$).[23,24] Within the framework of the drift-diffusion model, we may even estimate the space charge potential from the relaxation frequencies ω_i of the bulk arc (b) and the interfacial space charge (sc) arc[25,26] according to

$$\frac{\omega_b}{\omega_{sc}} = \frac{\exp(e\Delta\varphi/kT)}{2e\Delta\varphi/kT} \quad (8)$$

From the spectra, we obtain 845 mV at 450 °C and thus a realistic value with regard to the open circuit voltage of the illuminated PV cell at the same temperature (778 mV).

The spectrum changes drastically under illumination: Figure 7b displays the impedances measured at 400–500 °C under short-circuit condition. The high frequency arc is now outside the measurable frequency range, due to a strong decrease of its resistance and thus strong increase of its relaxation frequency. The resistance of the illuminated $SrTiO_3$ single crystal is drastically decreased to ≈4% of its original value at 450 °C. However, it is no longer significantly temperature dependent. From this we conclude that photoconductivity is strongly increased in the entire $SrTiO_3$ single crystal. Possibly the recombination of the generated electronic charge carriers in $SrTiO_3$ is sufficiently slow to "flood" the entire single crystal with electrons.

Transmission spectra of a $SrTiO_3$ single crystal and band gaps estimated from 50% of the maximum transmittance are shown in **Figure 8**. At room temperature 3.18 eV are found, in good agreement with the indirect band gap reported in literature (3.2 eV)[27,28] while at 500 °C the band gap is reduced to 2.78 eV. Hence, $SrTiO_3$ strongly absorbs the UV light used here (365 nm ⇒ 3.39 eV). (The indirect band gap of Sr-doped $LaCrO_3$ at room temperature is ≈2.8 eV[29,30] but varies with dopant concentration; this material was recently suggested as a p-type transparent conducting oxide.[31]) The size of the low frequency arc drastically decreases upon UV light by about two orders of magnitude at 450 °C. The corresponding total AC resistance of the illuminated PV cell (i.e., the low frequency intercept $R_{PV,AC,ill}$) is also included in Figure 6a and is in acceptable agreement with the differential resistance determined from the *I–V* curve close to short-circuiting condition.

A similar analysis can be made for the resistance of the EC part of the photoelectrochemical cell. For symmetrical gas supply, the entire voltage $U_{PEC} = U_{EC}$ is consumed by the different contributions to the overpotential of the electrochemical cell and thus a resistance can be calculated from

$$R_{EC,PEC} = \frac{U_{PEC}}{I_{PEC}} \quad (9)$$

Figure 6b displays the corresponding values for the illuminated PEC cell. Those are strongly temperature dependent and decrease from ≈900 Ω at 400 °C to 100 Ω at 500 °C. This strong temperature dependence (reflecting an activation energy of ≈1 eV) is not surprising, taking into account that temperature dependent processes are involved, namely ion conduction in zirconia and oxygen reduction/production at LSF electrodes.

In order to get more details on the main contributor to this internal EC resistance, again impedance spectroscopic studies were performed. Figure 7c shows spectra measured before and

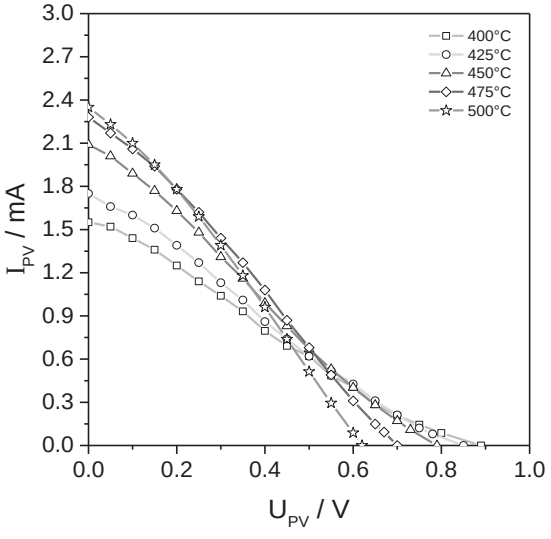

Figure 5. *I–V* characteristics of the PV cell solely, obtained by measuring U_{PV} and I_{PV} for different loads and temperatures from 400 °C to 500 °C ($T = T_{dark}$).

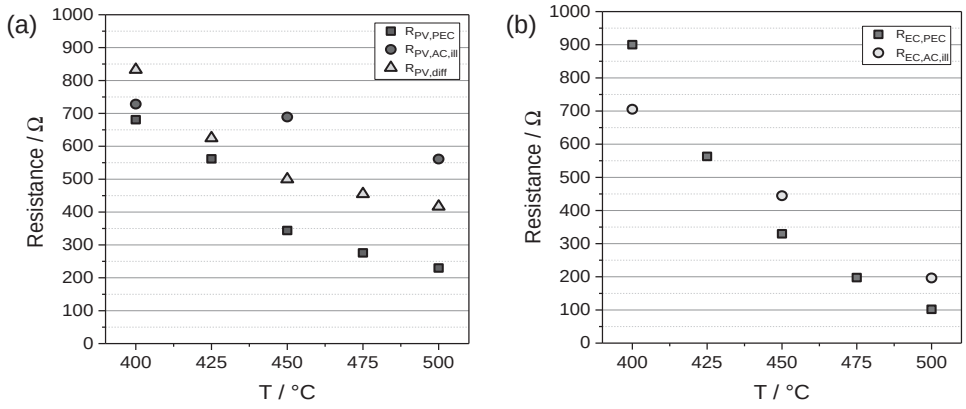

Figure 6. a) Temperature dependent resistances of the PV cell in the operating PEC cell ($R_{PV,PEC}$, $T = T_{dark}$), the corresponding total AC resistance of the illuminated PV cell ($R_{PV,AC,ill}$, $T = T_{UV}$) and the approximate differential resistances $R_{PV,diff}$ ($T = T_{UV}$) obtained by linearizing the *I–V* curves at temperatures between 400 and 500 °C. b) Temperature dependent resistances $R_{EC,PEC}$ calculated from U_{PEC}/I_{PEC} ($T = T_{dark}$) of the illuminated PEC cell and the total AC resistances of the illuminated cell ($R_{EC,AC,ill}$, $T = T_{UV}$) at temperatures between 400 and 500 °C.

during illumination of the short-circuited PEC cell at 450 °C. In both cases the spectrum consists of a high frequency intercept, a small intermediate frequency arc, and a large distorted low frequency arc. The capacitance of the intermediate frequency arc is much larger than a typical bulk capacitance of zirconia, indicating that it is either due to grain boundaries in TZP or an interfacial electrode effect. The high frequency intercept is largely due to ion conduction in the bulk (grains) of TZP; the conductivity calculated from the corresponding resistance (≈3.1×10^{-4} S cm^{-1}) fits well to the ionic conductivity of TZP reported in literature (≈(3–4) $\times 10^{-4}$ S cm^{-1}).[32,33] The low frequency arc has the typical half tear drop shape of porous mixed conducting electrodes in oxygen atmosphere[34] and is attributed to the electrochemical oxygen exchange reaction in the LSF electrodes.

Measurements upon illumination lead to much lower values of the LSF electrode related resistance, an effect that can be attributed to the nonlinearity of electrode processes in solid-state electrochemical cells. The total AC resistance of the cell ($R_{EC,AC,ill}$) is in the same range as the DC resistance $R_{EC,PEC}$ of the operating cell calculated from Equation (9), though less temperature dependent. Differences are most probably again due to the nonlinearity of the electrode resistances. The size of the high frequency intercept varies slightly despite nominally identical temperature of dark and illuminated PEC cell. This is attributed to a slight difference between the UV light induced heating of the thermocouple and of the sample itself (see Section 5).

From this analysis, we get also information on the cell component that is most critical under PEC cell operation. In accordance with Equations (7) and (9), the ratio

$$\frac{R_{PV,PEC}}{R_{EC,PEC}} = \frac{U_{PV,OC}}{U_{PEC}} - 1 \quad (10)$$

is a measure of the relative importance of the two internal resistances. **Figure 9** displays this ratio for different temperatures. At 400 °C, the EC cell contributes slightly more to the overall resistance than the PV cell; at these temperatures significant improvement could be made by optimizing the oxygen exchanging electrodes of the EC cell. At 500 °C, on the other hand, the electrochemical cell is already much less resistive than the PV cell. At this temperature, a reduction of the internal resistance of the PV cell would be most efficient. Reduction of the $SrTiO_3$ thickness may help, but also different doping of either $SrTiO_3$ or LSCr could be used to optimize performance and to achieve even higher voltages. Combining all these measures could ultimately enable a water splitting photoelectrochemical cell based on high-temperature solid-state components.

4. Conclusions

Combination of a highly Sr-doped $LaCrO_3$ thin film and a $SrTiO_3$ single crystal leads to a high-temperature photovoltaic cell with open circuit voltages up to >900 mV at 400 °C. When stacking this photovoltaic cell with a solid-state electrochemical cell, photo-powered oxygen pumping from low to high oxygen partial pressures becomes possible. Pumping currents of ≈1 mA cm^{-2} are realized and this causes a significant lowering of the oxygen content in the low oxygen pressure compartment of the PEC cell. Hence, the proof of concept for solar to fuel conversion by high-temperature solid-state electrochemical cells has been established. The measured voltages could be attributed to different internal resistances in the PEC cell or a Nernst voltage. Already moderate improvements of the cell are expected to lead to voltages and currents that allow water splitting in a steam-based high-temperature photoelectrochemical cell.

5. Experimental Section

The photoelectrochemical cell sketched in Figure 1a was prepared as follows: In a first step, a 475 nm thin layer of $La_{0.8}Sr_{0.2}CrO_3$ (LSCr) was deposited on a nominally undoped $SrTiO_3$ (100) single crystal (Crystec GmbH, Germany, 0.5 mm thickness, 10 × 10 mm^2) by pulsed laser deposition. The deposition time was 30 min (18 000 pulses) with the laser operating at a pulse energy of 400 mJ (at the laser) and a repetition

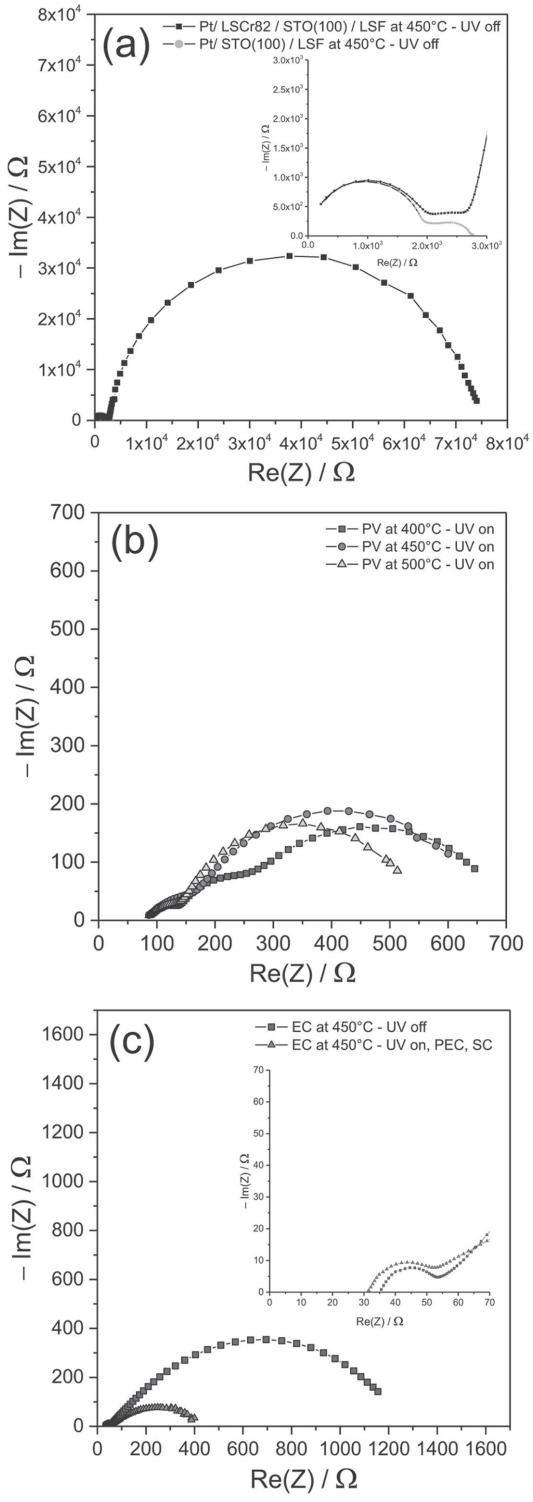

Figure 7. a) Impedance spectrum of the dark PV cell at 450 °C; the large arc is caused by the $SrTiO_3$/LSCr interface. The inset shows a magnification of the spectrum part caused by the $SrTiO_3$ single crystal and the spectrum of a $SrTiO_3$ single crystal with Pt instead of the LSCr as top electrode. b) Spectra of the illuminated PV cell measured at 400–500 °C ($T = T_{UV}$) under short-circuit condition. c) Impedance spectra of the EC cell before and during illumination of the short-circuited PEC cell at 450 °C ($T = T_{UV}$ for UV on and $T = T_{dark}$ for UV off).

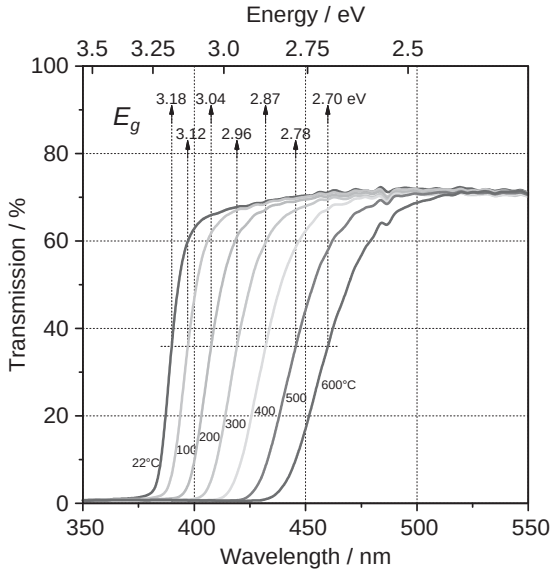

Figure 8. Wavelength dependent transmission of light through a $SrTiO_3$ single crystal (0.5 mm thickness) as function of temperature measured in air. Band gap energies E_g are deduced from half maximum transmission and are also indicated.

rate of 10 Hz. The LSCr material for the target was obtained from American Elements, LA, USA, pressed and sintered at 1200 °C for 12 h with a heating and cooling rate of 10 °C min^{-1}. A SEM cross section image of a LSCr layer on $SrTiO_3$ is shown in Figure 1b. On top of this layer, a Pt current collector grid (stripe width: 10 µm, stripe distance: 40 µm, Pt coverage of 23%) was prepared by sputter deposition and a subsequent lift-off photolithographic process.

In a second step, a symmetrical zirconia-based electrochemical cell was prepared: On a TZP substrate (KERAFOL Keramische Folien GmbH, 3 mol% Y_2O_3, 300 µm thickness, 2 cm in diameter) two porous mixed conducting LSF electrodes were deposited from a paste. For this purpose, LSF powder from Sigma-Aldrich, Germany was ground with 5 mg ethyl cellulose and mixed with 85 mg terpineol ($C_{10}H_{18}O$) per 0.15 g powder. In a final step, the $SrTiO_3$ single crystal with LSCr

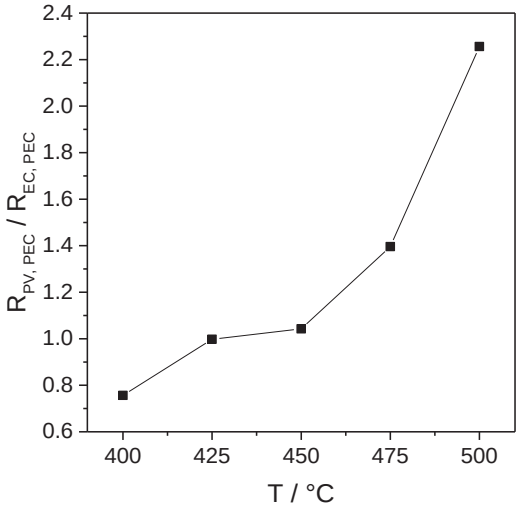

Figure 9. Ratio of the two PEC cell internal resistances, i.e., of the PV cell resistance $R_{PV,PEC}$ and the EC cell resistance $R_{EC,PEC}$ for temperatures between 400 and 500 °C ($T = T_{dark}$).

top layer was placed on the electrochemical cell and the entire oxide stack was heated to 850 °C for 5 h with a heating and cooling rate of 5 °C min^{-1} in ambient air in order to anneal the LSF electrodes and to mechanically link the two subsystems to form a single PEC cell. One LSF electrode thus acts as shared top electrode of the EC cell and bottom electrode of the PV cell. TZP was used as electrolyte because of its high mechanical stability.

The PEC cell was mounted in a tube furnace such that two different gas compartments resulted, see Figure 1c. The PV cell and the top LSF electrode of the EC cell were held in ambient air, while the bottom part of the EC cell (second LSF electrode) was exposed either to a 10 mL min^{-1} gas flow of nitrogen (with ≈600 ppm O_2 remaining oxygen due to nonideal gas tightness) or ambient air. The oxygen content in this gas was determined by an oxygen sensor (Rapidox 2100, Cambridge Sensotec Ltd., UK) positioned behind the gas outlet of the sample holder.

At temperatures between 400 and 500 °C, the PEC cell was illuminated by UV light using a 10 W light emitting diode (LED), (LED ENGIN, San Jose, USA) with 365 nm. Light guidance into the setup was established by a quartz bar (10 mm in diameter). The light intensity at the sample surface was ≈300 mW cm^{-2}. Electrical and electrochemical DC properties were measured with multimeters (DMM 2000, Keithely Instruments Inc., USA) as sketched in Figure 1. Additionally, impedance spectra of both the photovoltaic as well as the electrochemical part of the PEC cell were measured in two-point geometry by connecting the corresponding electrodes to an Alpha-A High Performance Frequency Analyzer from Novocontrol Technologies, Germany.

Upon illumination, the thermocouple (type K) positioned close to the sample, showed a slight increase of typically 6–8 °C. When appropriate, the set temperature of the heater was then decreased upon illumination such that the temperature measured by the thermocouple was the same as without illumination. It is indicated in all figures whether the given thermocouple temperature T refers to the dark (T_{dark}) or the illuminated (T_{UV}) case. The change of the TZP electrolyte resistance, measured by impedance spectroscopy, also allows an estimate of the temperature change upon UV illumination. Assuming an activation energy of 1 eV for ion conduction in zirconia we could deduce temperature increases of ≈5–10 °C, which is in excellent agreement with the changes indicated by the thermocouple.

Acknowledgements

The authors gratefully acknowledge funding by the Austrian Research Promotion Agency (FFG) under Project No. 838562. Furthermore, the authors are thankful to numerous colleagues of the Solid State Electrochemistry and Electroceramics Laboratory for fruitful scientific discussions and to the workshop of Institute for Energy Systems and Thermodynamics (Head: Prof. M. Haider) for excellent support in designing and manufacturing the setup for the photo(electro)chemical investigation, especially to A. Hofer and R. Steininger. Special thanks is also conveyed to Constantia Industries AG and NOVAPECC GmbH for financial support.

Received: August 25, 2015
Revised: October 12, 2015
Published online: November 19, 2015

[1] S. Licht, B. Wang, S. Ghosh, H. Ayub, D. Jiang, J. Ganley, *J. Phys. Chem. Lett.* **2010**, *1*, 2363.
[2] M. Uzunoglu, O. Onar, M. Alam, *Renewable Energy* **2009**, *34*, 509.
[3] T. L. Gibson, N. A. Kelly, *Int. J. Hydrogen Energy* **2010**, *35*, 900.
[4] O. Khaselev, J. A. Turner, *Science* **1998**, *280*, 425.
[5] A. Fujishima, K. Honda, *Nature* **1972**, *238*, 37.
[6] T. Ohnishi, Y. Nakato, H. Tsubomura, *Ber. Bunsenges. Phys. Chem.* **1975**, *79*, 523.
[7] J. Mavroides, J. Kafalas, D. Kolesar, *Appl. Phys. Lett.* **1976**, *28*, 241.
[8] J. Nowotny, C. Sorrell, T. Bak, L. Sheppard, *Solar Energy* **2005**, *78*, 593.
[9] G. Wang, H. Wang, Y. Ling, Y. Tang, X. Yang, R. C. Fitzmorris, C. Wang, J. Z. Zhang, Y. Li, *Nano Lett.* **2011**, *11*, 3026.
[10] A. Valdes, J. Brillet, M. Grätzel, H. Gudmundsdottir, H. A. Hansen, H. Jonsson, P. Klüpfel, G.-J. Kroes, F. Le Formal, I. C. Man, *Phys. Chem. Chem. Phys.* **2012**, *14*, 49.
[11] F. E. Osterloh, *Chem. Mater.* **2008**, *20*, 35.
[12] J. Gan, X. Lu, Y. Tong, *Nanoscale* **2014**, *6*, 7142.
[13] P. Haueter, S. Moeller, R. Palumbo, A. Steinfeld, *Sol. Energy* **1999**, *67*, 161.
[14] M. Roeb, C. Sattler, R. Klüser, N. Monnerie, L. de Oliveira, A. G. Konstandopoulos, C. Agrafiotis, V. Zaspalis, L. Nalbandian, A. Steele, *J. Sol. Energy Eng.* **2006**, *128*, 125.
[15] S. Abanades, G. Flamant, *Sol. Energy* **2006**, *80*, 1611.
[16] W. C. Chueh, C. Falter, M. Abbott, D. Scipio, P. Furler, S. M. Haile, A. Steinfeld, *Science* **2010**, *330*, 1797.
[17] H. Ishihara, H. Kaneko, N. Hasegawa, Y. Tamaura, *J. Sol. Energy Eng.* **2008**, *130*, 044501.
[18] X. Ye, J. Melas-Kyriazi, Z. A. Feng, N. A. Melosh, W. C. Chueh, *Phys. Chem. Chem. Phys.* **2013**, *15*, 15459.
[19] F. Horikiri, T. Ichikawa, L. Q. Han, A. Kaimai, K. Yashiro, H. Matsumoto, T. Kawada, J. Mizusaki, *Jpn. J. Appl. Phys.* **2005**, *44*, 8023.
[20] G. Walch, A. K. Opitz, S. Kogler, J. Fleig, *Monatsh. Chem.* **2014**, *145*, 1055.
[21] I. Denk, W. Münch, J. Maier, *J. Am. Ceram. Soc.* **1995**, *78*, 3265.
[22] A. Rothschild, W. Menesklou, H. L. Tuller, E. Ivers-Tiffee, *Chem. Mater.* **2006**, *18*, 3651.
[23] G. M. Choi, H. L. Tuller, *J. Am. Ceram. Soc.* **1988**, *71*, 201.
[24] R. A. De Souza, V. Metlenko, D. Park, T. E. Weirich, *Phys. Rev. B* **2012**, *85*, 174109.
[25] J. Fleig, S. Rodewald, J. Maier, *J. Appl. Phys.* **2000**, *87*, 2372.
[26] H. K. Heinisch, *Semiconductor Contacts*, Clarendon, Oxford **1984**, p. 84.
[27] M. Cardona, *Phys. Rev.* **1965**, *140*, A651.
[28] K. Van Benthem, C. Elsässer, R. French, *J. Appl. Phys.* **2001**, *90*, 6156.
[29] K. Maiti, D. Sarma, *Phys. Rev. B* **1996**, *54*, 7816.
[30] P. V. Sushko, L. Qiao, M. Bowden, T. Varga, G. J. Exarhos, F. K. Urban III, D. Barton, S. A. Chambers, *Phys. Rev. Lett.* **2013**, *110*, 077401.
[31] K. H. Zhang, Y. Du, A. Papadogianni, O. Bierwagen, S. Sallis, L. F. Piper, M. E. Bowden, V. Shutthanandan, P. V. Sushko, S. A. Chambers, *Adv. Mater.* **2015**, *27*, 5191.
[32] N. Bonanos, R. Slotwinski, B. Steele, E. Butler, *J. Mater. Sci. Lett.* **1984**, *3*, 245.
[33] B. Boukamp, T. Raming, A. Winnubst, H. Verweij, *Solid State Ionics* **2003**, *158*, 381.
[34] S. B. Adler, J. Lane, B. Steele, *J. Electrochem. Soc.* **1996**, *143*, 3554.